

Hard X-rays from Type II bursts of the Rapid Burster and its transition toward quiescence

N. Masetti¹, F. Frontera^{1,2}, L. Stella^{3,*}, M. Orlandini¹, A.N. Parmar⁴, S. Del Sordo⁵, L. Amati¹, E. Palazzi¹, D. Dal Fiume^{1,**}, G. Cusumano⁵, G. Pareschi⁶, I. Lapidus⁷, and R.A. Remillard⁸

¹ Istituto Tecnologie e Studio delle Radiazioni Extraterrestri, CNR, via Gobetti 101, 40129 Bologna, Italy

² Dipartimento di Fisica, Università di Ferrara, via Paradiso 11, 44100 Ferrara, Italy

³ Osservatorio Astronomico di Roma, via Frascati 33, 00040 Monteporzio Catone, Italy

⁴ Astrophysics Division, Space Science Department of ESA, ESTEC, Postbus 299, 2200 AG Noordwijk, The Netherlands

⁵ Istituto di Fisica Cosmica ed Applicazioni all'Informatica, CNR, via La Malfa 153, 90146 Palermo, Italy

⁶ Osservatorio Astronomico di Brera, via Bianchi 46, 23807 Merate, Italy

⁷ McKinsey & Co., Inc., No. 1 Jermyn Street, London SW1Y 4UH, UK

⁸ Center for Space Research and Department of Physics, Massachusetts Institute of Technology, 77 Massachusetts Avenue, Cambridge, MA 02139, USA

Received 13 June 2000 / Accepted 29 August 2000

Abstract. We report on 4 *BeppoSAX* Target Of Opportunity observations of MXB 1730–335, the Rapid Burster (RB), made during the 1998 February–March outburst. In the first observation, approximately 20 days after the outburst peak, the X–ray light curve showed Type II bursts at a rate of 43 hr^{−1}. Nine days later, during the second *BeppoSAX* pointing, only 5 Type II bursts were detected at the beginning of the observation. During the third pointing no X–ray bursts were detected and in the fourth and final observation the RB was not detected at all. Persistent emission from the RB was detected up to 10 keV during the first three pointings. The spectra of the persistent and bursting emissions below 10 keV were best fit with a model consisting of two blackbodies. An additional component (a power law) was needed to describe the 1–100 keV bursting spectrum when the persistent emission was subtracted. To our knowledge, this is the first detection of the RB beyond 20 keV. We discuss the evolution of the spectral parameters for the bursting and persistent emission during the outburst decay. The light curve, after the second *BeppoSAX* pointing, showed a steepening of the previous decay trend, and a sharper decay rate leading to quiescence was observed with *BeppoSAX* in the two subsequent observations. We interpret this behaviour as caused by the onset of the propeller effect. Finally, we infer a neutron star magnetic field $B \sim 4 \times 10^8$ Gauss.

Key words: stars: individual: MXB 1730–335 – stars: neutron – X-rays: bursts – X-rays: general – X-rays: stars

1. Introduction

The Rapid Burster (MXB 1730–335; hereafter RB) is a well known and extensively studied low mass X–ray binary (LMXRB; see the recent review by Lewin et al. 1995) located in the globular cluster Liller 1 at a distance of ~ 8 kpc (Ortolani et al. 1996). It is a recurrent transient with outbursts which last for few weeks followed by quiescent intervals which generally last for ~ 6 months. Recently, a likely radio counterpart to the RB was observed by Moore et al. (2000) during several X–ray outbursts.

The RB is unique among LMXRBs in that it displays two different kinds of X–ray bursts: Type I bursts, which are typical of many LMXRBs with low-magnetic field neutron stars (NS) and Type II bursts. The former events are interpreted as due to nuclear burning of accreted material onto the surface of the NS; Type II bursts, instead, probably result from spasmodic accretion onto the NS surface (e.g. Lewin et al. 1995). Until 1996, the RB was the only X–ray source from which Type II events were detected. Now another transient X–ray source, GRO J1744–28, is known to show hard X–ray bursts, that likely have the same origin of the RB Type II bursts (Kouveliotou et al. 1996). The NS nature of GRO J1744–28 has been clearly established from the observation in its X–ray emission of coherent 0.467 s pulsations (Finger et al. 1996).

The RB shows a variety of emission modes. At some times it appears as a typical low magnetic field LMXRB with persistent emission (PE) and Type I bursting emission (BE); but there are times when both Type I and Type II BE are observed, and times with only Type II BE. In the presence of Type II bursts only, the PE is well visible after long ($\gtrsim 30$ s) events, but is weak or absent during short Type II events. The time behaviour of the PE between Type II bursts, when it is observable, is complex with dips (before and after Type II burts), humps, glitches, bumps

Send offprint requests to: N. Masetti (masetti@tesre.bo.cnr.it)

* Affiliated to International Center for Relativistic Astrophysics

** Deceased on August 5, 2000

(Lubin et al. 1993) and periodicities known as ‘ringing tail’ observed shortly after long Type II bursts (Lubin et al. 1992).

Type II bursts have been observed with durations between ~ 3 s and 640 s: the shortest events (less than ~ 20 s) show a sharp rise and a decay with multiple peaks (‘ringing’), instead the longer events are flat topped. Their time behaviour is like that of a relaxation oscillator: their fluence E is roughly proportional to the time interval, Δt , to the following burst (Lewin et al. 1976).

Quasi-periodic oscillations (QPOs) with centroid frequencies in the range from ~ 2 to ~ 7 Hz were observed in Type II bursts; the centroid frequency was found to be anti-correlated with the burst peak flux (see review by Lewin et al. 1995). Also in the PE QPOs were observed with centroid frequencies from ~ 0.04 to ~ 4.5 Hz with no frequency–intensity correlation, a repetitive pattern from ~ 4 Hz to to ~ 2 Hz, and a positive correlation with spectral hardness (Stella et al. 1988).

The spectral properties of the Type II BE and of the PE have been extensively investigated in the X–ray energy band up to about 20 keV. Some authors (Marshall et al. 1979; Barr et al. 1987) found that Type II burst spectra were well fit by a blackbody (BB) spectrum with $kT \sim 1.5$ –2 keV, while Stella et al. (1988), analyzing long Type II bursts, found that the best fit was obtained with an unsaturated Comptonization model ($N(E) \propto E^{-\Gamma} \exp(-E/kT)$, with $\Gamma \sim 0.7$ and $kT \sim 2.6$ keV for 1.5–2 min events). Instead, a two-component blackbody (2BB) plus a power law (PL) provided the best fit to the spectra between 2 and 20 keV (Guerriero et al. 1999). The unsaturated Comptonization model was found to describe well the PE spectra (Barr et al. 1987; Stella et al. 1988), with $\Gamma \sim -0.06$ and $kT \sim 2.8$ keV in the time periods after 1.5–2 min Type II events (Stella et al. 1988). Instead Guerriero et al. (1999) found that the PE is well described by the same model used for the Type II bursts (i.e. 2BB+PL). An observation of the source in quiescence with the ASCA satellite provided a positive detection with a 2–10 keV luminosity of $(1.9_{-0.6}^{+1.3}) \times 10^{33}$ erg s $^{-1}$, for a distance of 8 kpc and an hydrogen column density of 1×10^{22} cm $^{-2}$ (Asai et al. 1996).

Up to now, a detailed study of the evolution of the spectral properties and the decay profile to quiescence of the RB has never been performed. In addition, the high-energy emission from the source is still poorly known (see, e.g., Claret et al. 1994). In order to address these issues, a series of observations was performed during the 1998 February–March outburst (Fox et al. 1998) with the *BeppoSAX* satellite (Boella et al. 1997a). In Sect. 2 we describe the observations, in Sect. 3 we present the spectral results, while in Sect. 4 we discuss them and the source transition to quiescence together with their implications.

2. Observations

The RB was observed with the *BeppoSAX* Narrow Field Instruments (NFIs) four times as a Target Of Opportunity (TOO). The NFIs include the Low-Energy Concentrator Spectrometer (LECS: 0.1–10 keV; Parmar et al. 1997), two Medium-Energy Concentrator Spectrometers (MECS: 1.5–10 keV;

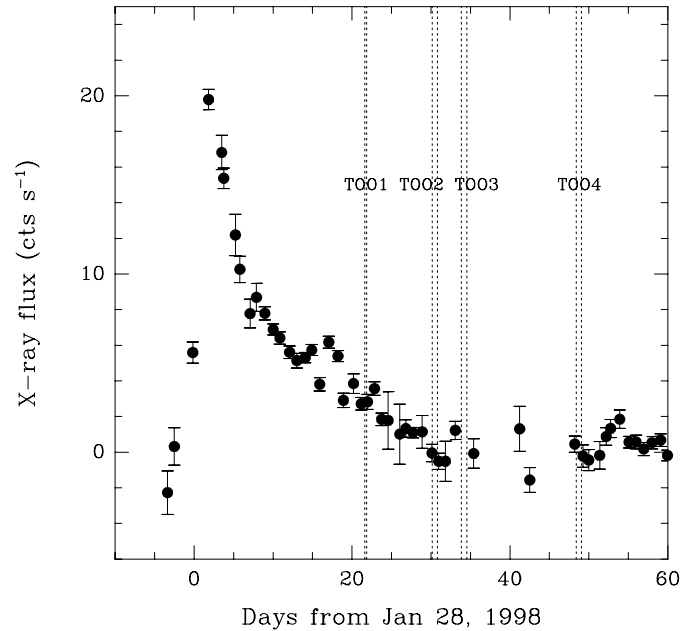


Fig. 1. *R-XTE/ASM* 2–10 keV light curve of the 1998 February–March outburst of the RB. The vertical dashed lines indicate the times of the 4 *BeppoSAX* TOO observations

Boella et al. 1997b), and the Phoswich Detection System (PDS: 15–300 keV; Frontera et al. 1997). The two MECS consist of grazing incidence telescopes with imaging gas scintillation proportional counters in their focal planes. The LECS uses an identical concentrator system as the MECS, but utilizes an ultra-thin entrance window and a driftless configuration to extend the low-energy response down to 0.1 keV. The LECS and the MECS have a circular field of view with diameter 37' and 56', respectively. The PDS (field of view of $\sim 1^\circ.3 \times \sim 1^\circ.3$ FWHM) consists of four independent detection units arranged in pairs, each one having a separate rocking collimator.

Table 1 reports the log of the TOO observations presented in this paper. They spanned just over one month (from February 18 to March 18) and caught the object during different emission modes and flux levels as it was decaying from an X–ray intensity of about 20% that of the outburst peak down to quiescence. Fig. 1 shows the 2–10 keV light curve obtained with the *All-Sky Monitor* (ASM) onboard the *Rossi X-ray Timing Explorer* (*R-XTE*) satellite¹. Also shown in Fig. 1 are the times of the four *BeppoSAX* observations.

Due to the presence of a strong and variable X–ray source, 4U 1728–34 (=GX 354–0, located $\sim 30'$ away from the RB), a special observation strategy for the latter instrument was adopted in order to minimize the contamination from this source: the PDS rocking collimators were offset by 40' along a direction opposite from that of 4U 1728–34. Unfortunately, due to an incorrect instrumental setting, these collimators did not move during TOO2 and TOO3. Thus only the LECS and MECS data are usable for these two observations.

¹ *R-XTE/ASM* light curves of X–ray sources are available at <http://space.mit.edu/XTE/asmlc/>.

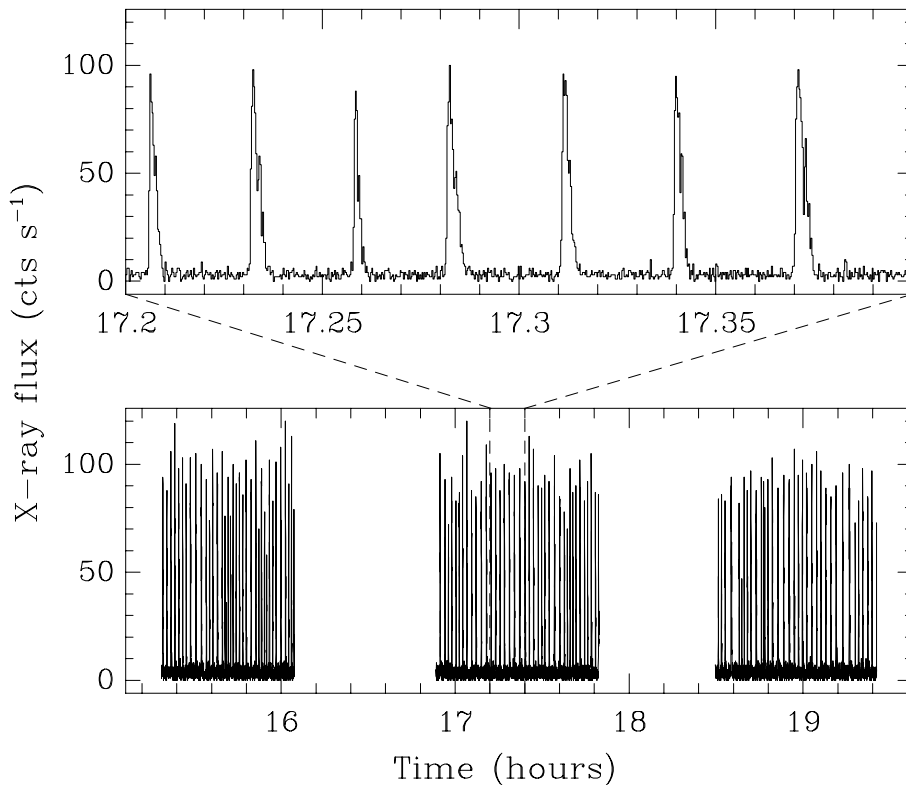


Fig. 2. MECS 2–10 keV light curve of TOO1. Times are expressed in hours from 0 UT of 1998 February 18. On top of the figure, the enlargement of the central part of the light curve is shown

Table 1. *BeppoSAX* observation log of the TOOs presented in this paper

TOO	Outburst day	Start day (1998)	Start time (UT)	Duration (ks)	Exposure (MECS; ks)	2–10 keV MECS count rate (s^{-1})
1	21	Feb 18	15:17	17.5	9.5	7.88
2	30	Feb 27	03:55	57.1	27.0	1.01
3	33	Mar 2	19:57	61.5	29.8	0.15
4	48	Mar 17	09:52	56.7	31.3	<0.02

During the last observation the RB, very faint at that time, was not detected with the NFIs. Contamination from 4U 1728–34, which was unusually intense at the time, adversely affected the sensitivity of all the NFIs during this observation. This issue is analyzed in more detail in Sect. 3.4 of this paper.

3. Data analysis and results

Good NFI data were selected from intervals when the elevation angle above the Earth limb was $>5^\circ$ and when the instrument functioning was nominal. The SAXDAS 2.0.0 data analysis package (Lammers 1997) was used for the LECS and MECS. The PDS data reduction was performed using XAS version 2.1 (Chiappetti & Dal Fiume 1997). The LECS and MECS events from the RB were extracted from circular regions with radii between $3'$ and $8'$, centred on the source position. These extraction radii were chosen case by case in order to optimize the signal-to-noise ratio for different X-ray intensities of the RB. The MECS exposure times are given in Table 1. Background subtraction for the two imaging instruments was performed us-

ing standard files, while the background for the PDS data was evaluated from offset fields.

The 2–10 keV MECS light curves of TOO1 and TOO2, with a time binning of 1 s, are shown in Fig. 2 and Fig. 3, respectively. The gaps in the light curves are due to non-observing intervals during Earth occultations and during passages through the South Atlantic Geomagnetic Anomaly. The mean source count rates with the MECS are given in Table 1.

The LECS and MECS spectra were rebinned to oversample by a factor 3 of the FWHM of the energy resolution, and having a minimum of 20 counts per bin such that the χ^2 statistics could reliably be used. The PDS spectra were rebinned using the standard techniques in SAXDAS. Data were selected in the energy ranges where the instrument responses were well determined: 0.5–8.0 keV for the LECS, 1.8–10 keV for the MECS, and 15–100 keV for the PDS. The only exception to this choice was during TOO1, in which LECS data were selected between 1 and 8 keV due to poor signal-to-noise ratio below 1 keV. We used the package XSPEC v10.0 (Arnaud 1996) for the spectral fitting. In the broadband fits, normalization factors were applied to the LECS and PDS spectra following the cross-calibration tests be-

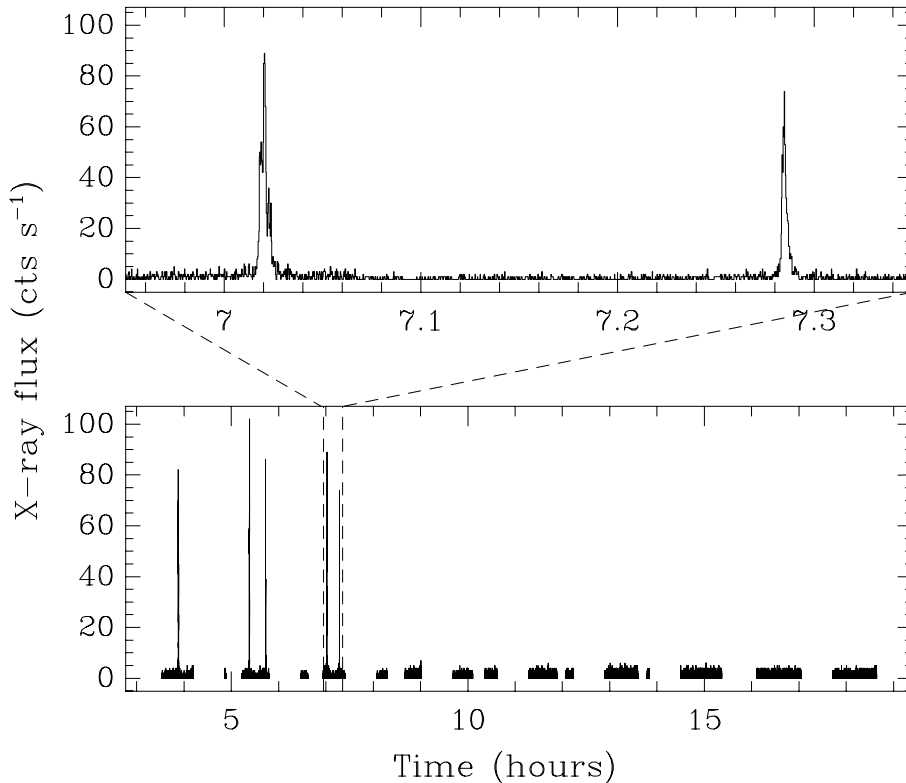


Fig. 3. MECS 2–10 keV light curve of TOO2. Times are expressed in hours from 0 UT of 1998 February 27. Note the marked reduction in bursting activity with respect to TOO1 (Fig. 2). On top of the figure, the enlargement of the section of the TOO2 light curve containing the last two bursts is shown

tween these instruments and the MECS (Fiore et al. 1999). For clarity of display, the spectra from multi-instrument fits (Figs. 5, 6 and 7) are shown normalized to the level of the MECS. The reported uncertainties throughout the paper are single parameter errors at 90% confidence level. For the luminosity estimates we will assume a distance to the RB of 8 kpc (Ortolani et al. 1996).

3.1. TOO1

During TOO1, the RB was in a state of strong bursting activity: indeed, the MECS light curve (Fig. 2) showed 113 X-ray bursts during 9.5 ks of good observation time, corresponding to an average rate of 43 bursts hr^{-1} . Their Type II character is apparent from the ‘ringing’ visible in their profiles and by the time between them. The RB appeared to be in the Phase II, Mode II of the classification by Marshall et al. (1979): all the events occurred almost regularly (at a time distance of about 100 s) and had short time durations (about 15 s). Also in the 0.1–2 keV LECS data these Type II bursts were visible. The total time-averaged 2–10 keV unabsorbed flux level during TOO1 was $8.2 \times 10^{-10} \text{ erg cm}^{-2} \text{ s}^{-1}$.

3.1.1. 1–10 keV spectrum of BE and PE

For the spectral analysis in the 1–10 keV energy range, the MECS TOO1 data, binned at 1 s, were divided into two subsets: PE (below 5 counts s^{-1}) and BE (above 5 counts s^{-1}). Then, LECS and MECS BE and PE spectra were accumulated using these two time windows. Given the small extraction radii used (4' for the MECS, 8' for the LECS), the high RB intensity level

and the low flux level of 4U 1728–34 at that time, the contamination from the latter source was negligible.

The BE 1–10 keV spectrum can be well fit ($\chi^2/\nu = 463/395$, where ν indicates the number of degrees of freedom in the fit) with a 2BB model, photoelectrically absorbed (the hydrogen column density was modeled using the Wisconsin cross sections as implemented in XSPEC; see Morrison & McCammon 1983). The same fitting model applies to the PE spectrum ($\chi^2/\nu = 217/203$). In Table 2 we show the fit results. The 2BB model was also used by Guerriero et al. (1999) to fit the *R-XTE/PCA* BE and PE spectra of the RB in the 2–20 keV band. These authors however noted that the PE between 10 and 20 keV was better fit by adding a PL component. In our 2–10 keV band spectra this was not necessary; but, when the data beyond 10 keV were considered (see Sect. 3.1.2), an additional component had to be added.

As it can be seen from Table 2, the BB temperatures did not significantly change for the PE and the BE, while the 2BB luminosities were much higher during BE than during PE. The column densities appeared also to be different for PE and BE spectra: $(1.5 \pm 0.3) \times 10^{22} \text{ cm}^{-2}$ and $(3.5 \pm 0.5) \times 10^{22} \text{ cm}^{-2}$, respectively. The increase of the N_{H} column density during the BE is apparent. The value obtained for the PE is consistent with the color excess $E(B - V)$ measured along the RB direction (Tan et al. 1991).

From the MECS 2–10 keV TOO1 observation we also computed the ratio, α , between the (unabsorbed) PE and BE fluences integrated over the TOO1 observation time. We found that $\alpha = 0.154 \pm 0.002$, that is about two orders of magnitude lower than the minimum value observed (~ 10) in the case of Type I X-

Table 2. Best-fit parameters for the TOO spectra. L is the unabsorbed luminosity in units of 10^{36} erg s^{-1} assuming a distance of 8 kpc

Model and parameter	TOO1			TOO2		TOO3
	1–10 keV BE	1–10 keV PE	1–100 keV BE – PE	1.8–10 keV BE	0.5–10 keV PE	0.5–10 keV PE
χ^2/ν	463/395	217/203	262/223	59/128	110/113	59/55
2BB:						
N_H ($\times 10^{22}$ cm $^{-2}$)	3.5 ± 0.5	1.5 ± 0.3	$4.9_{-1.1}^{+1.7}$	[4.0 ^a]	1.6 ± 0.3	$1.1_{-0.3}^{+0.4}$
kT_1 (keV)	0.46 ± 0.04	0.63 ± 0.06	$0.32_{-0.12}^{+0.23}$	$0.46_{-0.08}^{+0.10}$	0.65 ± 0.07	0.64 ± 0.09
L_1^{BB}	15_{-5}^{+6}	$0.85_{-0.06}^{+0.08}$	10_{-10}^{+22}	14_{-3}^{+4}	$0.32_{-0.03}^{+0.04}$	0.06 ± 0.01
R_1^{BB} (km)	51 ± 13	6.5 ± 1.3	90_{-80}^{+160}	48_{-19}^{+32}	3.7 ± 0.8	1.7 ± 0.5
kT_2 (keV)	1.64 ± 0.03	$1.72_{-0.17}^{+0.19}$	1.67 ± 0.04	$1.57_{-0.13}^{+0.19}$	$1.78_{-0.08}^{+0.10}$	$2.1_{-0.2}^{+0.4}$
L_2^{BB}	47 ± 0.8	$0.74_{-0.05}^{+0.06}$	40 ± 2	$24.2_{-1.6}^{+1.4}$	0.76 ± 0.03	$0.106_{-0.008}^{+0.011}$
R_2^{BB} (km)	7.1 ± 0.7	0.81 ± 0.17	6.3 ± 0.3	$5.6_{-1.3}^{+1.2}$	0.76 ± 0.08	$0.21_{-0.04}^{+0.07}$
+ power law:						
Γ			$3.1_{-0.4}^{+0.3}$			
K (ph keV $^{-1}$ cm $^{-2}$ s $^{-1}$ at 1 keV)			$3.3_{-2.5}^{+4.5}$			
+ Fe emission line:						
E_l (keV)			6.5 ± 0.2			
EW (eV)			100_{-60}^{+80}			
FWHM (keV)			$0.4_{-0.4}^{+0.3}$			
I_l ($\times 10^{-3}$ ph cm $^{-2}$ s $^{-1}$)			7_{-4}^{+5}			
L_{2-10} keV	43.5 ± 0.3	1.08 ± 0.02	47.3 ± 0.3	24.6 ± 0.9	0.78 ± 0.01	0.109 ± 0.002
L_{10-100} keV			7.2 ± 1.1			

^a fixed at the best fit value determined from the 1–10 keV BE spectrum of TOO1

ray bursts (Lewin et al. 1995). This result confirms the Type II character of the detected bursts.

3.1.2. 1–100 keV spectrum of the BE

During TOO1 the RB was also visible in hard X-rays (15–100 keV). However, due to the lower statistical quality of the data, the PDS light curve was much noisier and it was difficult to single out the bursts. In order to separate the BE from the PE, two PDS spectra (‘persistent’ and ‘bursting’) were accumulated using the time intervals of the bursts given by the MECS data. Given the residual contamination from 4U 1728–34, we only derived the high energy spectrum of the BE using as background level the count rate spectrum measured during the PE time intervals.

The combined LECS+MECS+PDS PE-subtracted BE spectrum in the 1–100 keV energy band is shown in Fig. 5. As it can be seen, the source was clearly detected at high energies. To our knowledge, this is the first time the RB is detected above 20 keV. A simple 2BB model did not clearly fit the data ($\chi^2/\nu = 326/228$), especially at high energies (>10 keV). A satisfactory fit ($\chi^2/\nu = 281/226$) was obtained by adding to the 2BB model a PL. The best fit parameters are given in Table 2.

We also tried to use, alternatively to the PL, a Comptonization model of soft photons in a hot thermal plasma (Titarchuk 1994; COMPTT model in XSPEC), by assuming seed photons

with temperature given by one of the two temperatures of the 2BB model. A fit quality ($\chi^2/\nu = 278/225$) similar to that achieved with the PL model was obtained, but electron temperature and optical depth of the comptonizing cloud were not constrained by the data ($kT_e \sim 20$ keV and $\tau \sim 0.4$, with large uncertainties). When the Comptonization model was used, the fit quality did not depend on the chosen seed photon temperature: both the cooler and the hotter BB photons provided fits of comparable quality. Also, disk and spherical geometries for the Comptonization resulted in equivalent fits.

The addition of a Fe K emission line to the 2BB+PL improved the fit ($\chi^2/\nu = 262/223$); the probability of a chance improvement, computed by means of an F-test, was quite low ($\sim 1 \times 10^{-3}$). The flux and energy centroid derived for the Fe K line (see Table 2) are consistent with the findings by Stella et al. (1988), while the width is lower by a factor ~ 3 . However Barr et al. (1987) gave an upper limit to the width of this line which is consistent with our measurement. No evidence of the same line was found in the 1–10 keV PE spectrum; however the flux was too low to allow a similar detection.

3.2. TOO2

During this observation the RB drastically reduced its bursting activity (see Fig. 3): only 5 bursts were detected at the beginning of the observation, with time duration of ~ 30 –40 s and time

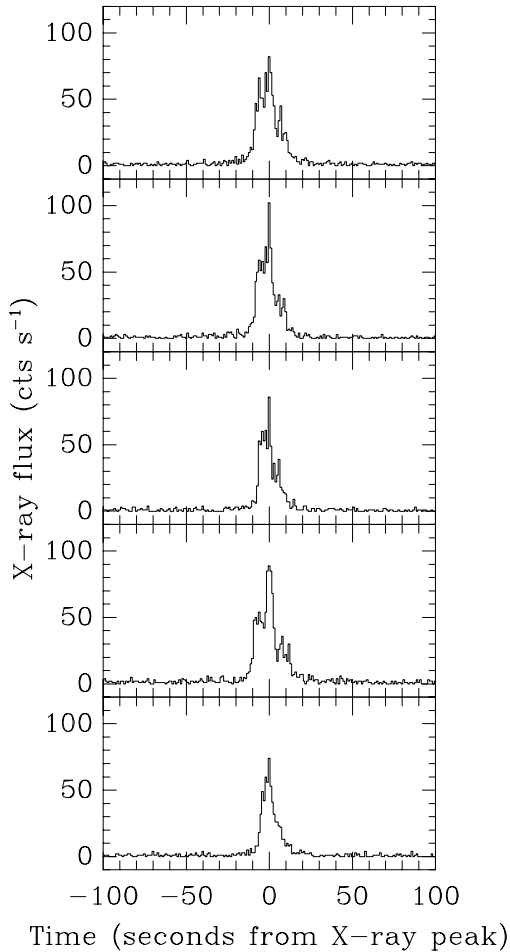


Fig. 4. 2–10 keV band light curves of the 5 bursts observed during TOO2. Times are expressed in seconds from the burst peak. Different shapes and lengths with respect to TOO1 bursts (see enlargement of Fig. 2) are apparent

distance among them spanning from ~ 20 to ~ 90 minutes. The general shape of these 5 bursts (Fig. 4) is similar each other and differs from those of TOO1 for the pre-maximum during their rise. This appears to be a sort of ‘hybrid’ shape between short (< 15 s) and long (1 min or more), flat-topped bursts (see, e.g., Lubin et al. 1992, 1993, and Guerriero et al. 1999).

The 2–10 keV flux level of the PE decreased by a factor 1.4, while the total time-averaged 2–10 keV unabsorbed flux (1.0×10^{-10} erg cm $^{-2}$ s $^{-1}$) decreased by a factor of about 8 with respect to TOO1.

The 2–10 keV α ratio between the (unabsorbed) PE and BE fluences integrated over the TOO2 observation time was 4.17 ± 0.15 , thus significantly higher than that found during TOO1, but lower than the minimum value measured in the case of Type I X-ray bursts. Given that some bursts might have been lost during the source occultation by the Earth, we have also computed α for the first three orbits of TOO2, i.e. where the 5 bursts were seen. In this case, we found that $\alpha = 1.40 \pm 0.05$. This value is still higher than that found in TOO1, but lower than the minimum value measured in the case of Type I bursts.

The 1.8–10 keV spectrum of the BE in TOO2 was still consistent with the 2BB model with $kT_1 \sim 0.5$ keV and $kT_2 \sim 1.6$ keV, even though, due to the poor statistics particularly in the LECS and below 2 keV, we could not derive accurate parameter values. Therefore, to better constrain the main parameters of the model, we fixed the N_H value to that obtained from the spectral fit of the TOO1 1–10 keV BE. The results of the TOO2 BE fit are reported in Table 2.

The PE also (see Fig. 6) was best fit ($\chi^2/\nu = 110/113$) with a photoelectrically absorbed 2BB model (see Table 2) with $kT_1 = 0.65 \pm 0.07$ keV and $kT_2 = 1.78^{+0.10}_{-0.08}$ keV, although a photoelectrically absorbed bremsstrahlung model also gave an acceptable fit ($\chi^2/\nu = 122/115$). The 2BB temperatures of BE and PE did not appear to change significantly from the corresponding values measured during TOO1. No substantial improvement in the fit was seen if a PL or a Comptonization component was included. No indication for a Fe K emission line was present in the TOO2 data.

3.3. TOO3

During TOO3, 33 days from the outburst onset, the source further reduced its X-ray emission and no bursts were seen throughout the observation. The unabsorbed and time-averaged 2–10 keV flux, 1.4×10^{-11} erg cm $^{-2}$ s $^{-1}$, had decreased by a factor 7 with respect to TOO2.

The 0.5–10 keV spectrum of the PE is shown in Fig. 7. Again it was well fit ($\chi^2/\nu = 59/55$) with a photoelectrically absorbed 2BB model (see Table 2), with $kT_1 = 0.64 \pm 0.09$ keV and $kT_2 = 2.1^{+0.4}_{-0.2}$ keV. The temperature of the hotter component seemed to be marginally higher than the corresponding value observed in TOO2, while kT_1 was fully consistent with the value obtained during TOO2. A photoelectrically absorbed bremsstrahlung gave a poorer fit ($\chi^2/\nu = 70/57$). As in the case of TOO2, no Fe K emission line was detected.

3.4. TOO4

During this observation the RB was no longer visible in the LECS and MECS images. Instead, strong contamination due to stray light from 4U 1728–34 was apparent and extended up to the center of the MECS image, where the RB emission was especially located. 4U 1728–34 was particularly active during TOO4 and prevented us from getting a deep observation of the RB. The PDS data were excluded from the analysis of TOO4 data since it proved impossible to disentangle the RB emission from the contamination induced by 4U 1728–34.

Using the background level present in the extraction circle of the RB image, we evaluated the upper limit to the 2–10 keV count rate from the RB. The result of this analysis indicates that, assuming the best fit model spectrum of TOO3, an emission of 1.5×10^{-12} erg cm $^{-2}$ s $^{-1}$ from the RB would have been clearly detected at 3σ at the relevant position in the MECS field of view. Thus, we can conservatively consider this value as a 3σ upper limit to the RB X-ray emission in the 2–10 keV energy band.

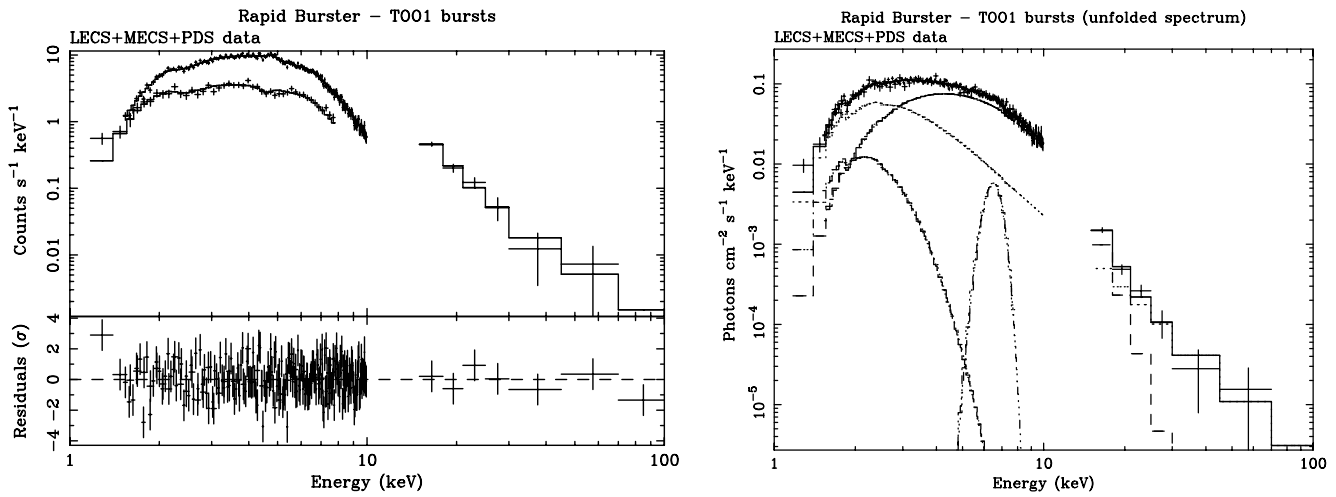


Fig. 5. TOO1 1–100 keV count rate (left panel) and photon (right panel) spectra of the total PE-subtracted BE. The fit corresponds to a photoelectrically absorbed two-component blackbody plus power law model plus an iron line at 6.5 keV

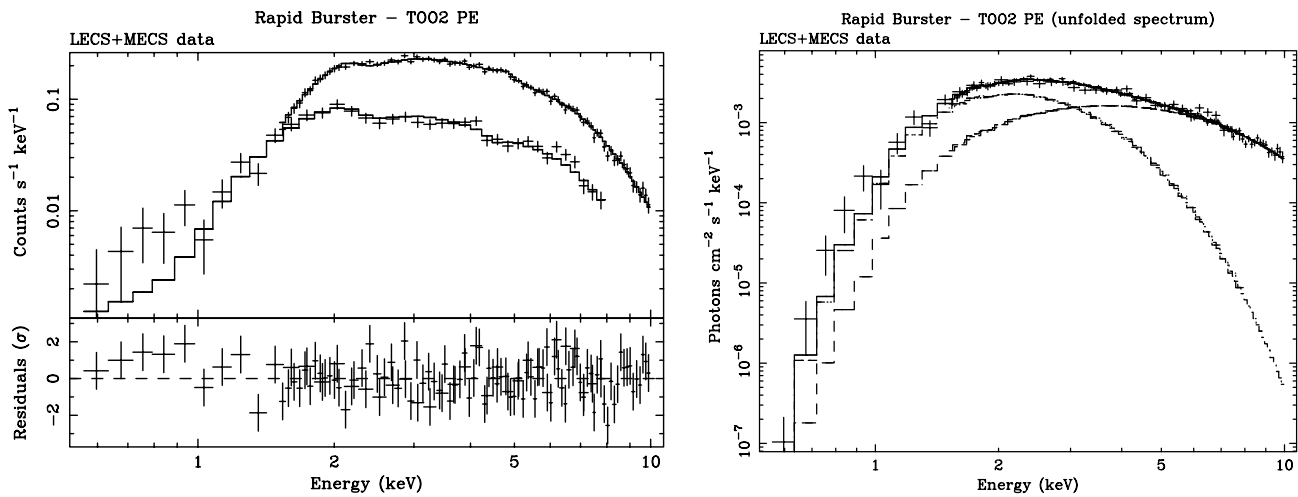


Fig. 6. TOO2 0.5–10 keV count rate (left panel) and photon (right panel) spectra of the PE. The fit corresponds to a photoelectrically absorbed two-component blackbody model

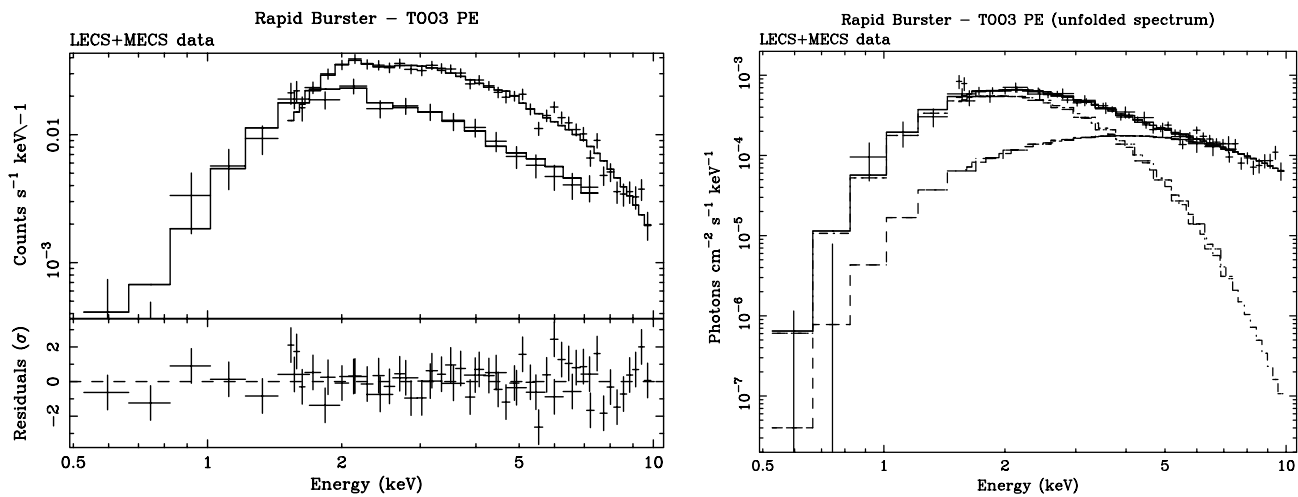


Fig. 7. TOO3 0.5–10 keV count rate (left panel) and photon (right panel) PE spectra. The fit corresponds to a photoelectrically absorbed two-component blackbody model

The corresponding 3σ upper limit to the 2–10 keV luminosity is $1.1 \times 10^{34} \text{ erg s}^{-1}$.

4. Discussion

The *BeppoSAX* observations of the RB have permitted us to detect for the first time high energy X-rays (>20 keV) from Type II bursts and to study the source in the late phase of the flux decay, from 21 to 48 days after the outburst onset. Type II bursts were detected in TOO1 and TOO2, corresponding to 21 and 30 days since the outburst start, while the PE was observed in all TOOs but the last observation, when the RB was not visible anymore.

4.1. Spectral properties of the Type II bursts and of the PE

The broad band (1–100 keV) PE-subtracted spectrum of the BE, measured during TOO1, is well described by a 2BB+PL model, with BB temperatures of ~ 0.3 and ~ 1.7 keV, while the photon index of the high energy PL component is ~ 3 . The presence of a high energy component is not apparent in the 1–10 keV spectrum, well described by a simple 2BB model. A thermal Comptonization model (Titarchuk 1994) also fits the high energy component of the BE PE-subtracted spectrum, but the thermal plasma parameters are not well constrained.

The presence of a high energy component is common in persistent low-luminosity LMXRBs (mainly X-ray bursters, see e.g. the review paper by Tavani & Barret 1997), and it is also seen during the outburst in some Soft X-ray Transients (SXTs) containing NSs (e.g., Aql X-1 and Cen X-4, see Campana et al. 1998). Instead this component is generally not observed in high-luminosity LMXRBs (Z-sources; see e.g. White et al. 1988). Only recently, thanks to *BeppoSAX*, evidence of high energy components in Z sources has been reported from some objects (Frontera et al. 1998; Masetti et al. 2000). This component has been interpreted in these sources as due to the presence, along with an accretion disk, of a cloud of hot electrons which Comptonize soft photons coming from the disk, similarly to what occurs in stellar mass black-hole candidates (Barret et al. 2000).

The BE spectrum (not PE-subtracted) below 10 keV during TOO1 and TOO2 is well fit with a 2BB model, in spite of a different shape of the burst time profiles as seen in these two *BeppoSAX* pointings. The 2BB temperatures of the BE do not appear to change from TOO1 to TOO2, as well as the cooler BB luminosity, while the hotter BB component changes its luminosity by a factor 2. This means that the BB radius of the hotter component is sensibly lower during TOO2 BE.

The PE, with decreasing intensity, has been detected up to 10 keV in all but the last TOO observations (see Table 2). Its spectrum is well fit by a 2BB model over the luminosity range over which the source could be studied with the LECS and the MECS (from TOO1 to TOO3). The temperatures of the two BB components do not change with time, except for a marginal evidence of an increase in the hotter component during TOO3. The BB luminosities instead do change. As a consequence, both

BB radii (see Table 2) decrease with time: R_1^{BB} from 6.5 to 1.7 km, and R_2^{BB} from 0.8 to 0.2 km.

Within the errors, PE and BE have hotter BB components with the same temperatures, while the temperature of the cooler BB component is slightly higher during PE than during BE (0.63 ± 0.03 keV against $0.43^{+0.04}_{-0.03}$ keV). During TOO1, the BB luminosities are however much different in the two source states: the BE/PE luminosity ratio of the hotter BB is 64 ± 5 during TOO1 and 32 ± 2 in TOO2, while that of the colder BB is 18 ± 7 in TOO1 and 44 ± 12 during TOO2. Also, in TOO1, during the BE the hotter BB component is brighter (by nearly a factor 3) than the cooler BB, while during the PE they have similar luminosities. In TOO2, instead, the latter ratio becomes ~ 2 due to the lower PE luminosity of the cooler BB.

On the basis of these features, a possible picture of the 2BB model (already discussed by Guerriero et al. 1999) is that the colder component originates from an accretion disk, while the hotter from the NS surface. A Comptonizing plasma cloud is the likely origin of the BE high energy component. The increase in luminosity of the colder BB component during the BE can be interpreted as an increase of the disk emitting surface (by a factor ~ 20 in TOO1 and ~ 40 in TOO2) as a consequence of the reduction of the inner radius of the accretion disk, while that of the hotter component could be due to an expansion in size (by a factor ~ 60 in TOO1 and ~ 30 in TOO2) of the NS surface that emits X-rays.

4.2. Outburst decay toward quiescence

Another relevant result of our observations is the determination, for the first time, of the source flux decay toward quiescence. In Fig. 8 we show the decay curve of the 1998 Feb-Mar outburst of the RB based on the *R-XTE/ASM* and *BeppoSAX* data. As it can be seen, starting from day 28 after the outburst onset, the flux decay becomes much faster than before: the e -folding decay time τ changes from $\tau_1 \sim 10$ days to $\tau_2 \sim 0.2$ days. This behaviour is reminiscent of the final evolution of dwarf novae outbursts (Osaki 1996) and of the transition to quiescence of the SXTs that harbour a low magnetic field NS (e.g., Aql X-1, Campana et al. 1998; SAX J1808.4-3658, Gilfanov et al. 1998) or a black hole (see the review by Tanaka & Shibazaki 1996). In the case of Aql X-1 (Campana et al. 1998) this time behaviour was interpreted as a consequence of the propeller effect (Illarionov & Sunyaev 1975). In the present case, the same effect can explain our observational results also. Indeed a magnetosphere may be present in the RB as consequence of the relaxation oscillator character of the Type II bursts recurrence behaviour (Lamb et al. 1977; Baan 1977, 1979) and low frequency QPOs detected in the BE and PE (Stella et al. 1988; Lewin et al. 1995). In the model by Baan (1977, 1979), a reservoir of matter floats on the top of the NS magnetosphere, partly supported by centrifugal forces. In the intervals between bursts, the magnetosphere becomes larger than the corotation radius. As matter accumulates on the magnetospheric boundary, this shrinks. When the magnetospheric radius becomes lower than a critical value at which gravity overcomes the centrifugal and

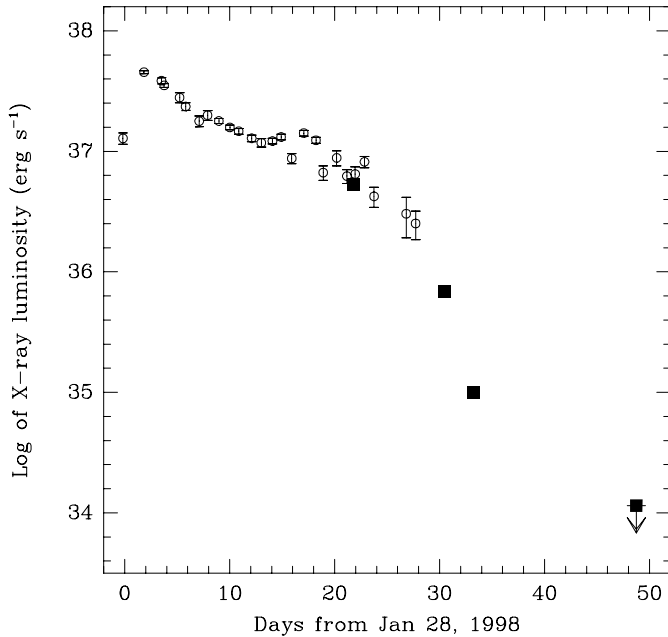


Fig. 8. Light curve of the 1998 February-March outburst of the RB. The filled squares are the *BeppoSAX* 2–10 keV fluxes derived using the best-fit model given in Table 2, while the open circles represent 3- σ detections of the RB taken from the *R-XTE/ASM* archive. The errors of the *BeppoSAX* measurements were not plotted since they are smaller than the corresponding symbols

magnetospheric forces, Type II bursts occur. This model is qualitatively in agreement with our observations. As long as we observed (in TOO1) Type II bursts, the flux decay was on the extrapolation of the earlier light curve. During TOO2, when we mainly observed PE (only 5 bursts at the beginning of the *BeppoSAX* pointing were detected), we found the first deviation. The sharper decrease of the PE intensity continued down to our quiescent luminosity upper limit.

In this scenario, the absence of Type II bursts in this decay phase is due to no accumulation of matter on the magnetospheric boundary, as consequence of a low mass accretion from the companion star. This fact leads to an increased magnetospheric radius. When the magnetospheric radius $R_m = 9.8 \times 10^5 \mu_{26}^{4/7} M_{1.4}^{1/7} (L_{38} R_6)^{-2/7}$ cm (μ_{26} is the magnetic dipole moment in units of 10^{26} Gauss cm³ and $M_{1.4}$ is the NS mass in units of $1.4 M_\odot$) becomes equal to the corotation radius $R_{cor} = 1.67 \times 10^8 P^{2/3} M_{1.4}^{1/3}$ cm (P is the spin period), accretion is inhibited (Stella et al. 1986). The corresponding minimum luminosity is given by $L_{min} \sim 4 \times 10^{36} B_8^2 P_{-3}^{-7/3}$ erg s⁻¹, where $B = B_8 10^8$ Gauss is the surface magnetic field of the NS, and $P = P_{-3} 10^{-3}$ ms is the NS spin period (NS mass M and radius R are assumed to be $1.4 M_\odot$ and 10^6 cm, respectively). Once accretion onto the NS surface is inhibited, as also discussed by Stella et al. (1994) and Campana et al. (1998), a lower accretion luminosity L_{cor} , corresponding to a gravitational potential energy of $GM\dot{M}_{min}/R_{cor}$, is released. It can be easily shown that $L_{cor} \sim 2 \times 10^{36} B_8^2 P_{-3}^{-3}$ erg s⁻¹, with the

same assumptions made for L_{min} (Campana et al. 1998). From Fig. 8, we can estimate $L_{min} \sim 3 \times 10^{36}$ erg s⁻¹.

On the other hand, Fox & Lewin (1999), from a timing analysis of *R-XTE* data from the RB, found two peaks in the power spectral density spectrum of the Type I BE, one at 154.9 ± 0.1 Hz and the other at 306.6 ± 0.1 Hz. Assuming the lower frequency as due to the spin period, from the estimated value of L_{min} we would obtain $L_{cor} \sim 6 \times 10^{35}$ erg s⁻¹. This is significantly lower than the luminosity measured during TOO2, which can be considered as a lower limit for L_{cor} . A higher value of L_{cor} (9×10^{35} erg s⁻¹) is expected in the case we assume as spin period that corresponding to the higher frequency reported by Fox & Lewin (1999). This spin period (3.3 ms) is more consistent with our results and implies a magnetic field $B \sim 4 \times 10^8$ Gauss, which then appears, on the basis of our luminosity data, the most likely value of B to be associated to the NS harboured in the system.

The contamination from 4U 1728–34 prevented us to draw conclusions on the quiescent luminosity from the RB. Our 3σ upper limit to this luminosity (1×10^{34} erg s⁻¹) is consistent with the luminosity level ($1.9_{-0.6}^{+1.2} \times 10^{33}$ erg s⁻¹) reported by Asai et al. (1996) during quiescence. The latter value is consistent with the minimum accretion luminosity (1.6×10^{33} erg s⁻¹) that can be emitted in the propeller regime ($\sim 2 \times 10^{34} B_8^2 P_{-3}^{-9/2}$ erg s⁻¹, Campana et al. 1998), even though the detected luminosity, as discussed by Asai et al. (1996), could be partially due to low-luminosity X-ray sources within the globular cluster Liller 1. An unbiased estimate of the RB quiescent luminosity is highly desirable to test the role of the propeller effect in quiescence.

Acknowledgements. We are grateful to P. Giommi for his help in the use of *SAXSIM* for the analysis of the TOO4 MECS data. *BeppoSAX* is a joint Italian and Dutch programme. This research was partly supported by the Italian Space Agency.

References

- Arnaud K.A., 1996, In: Jacoby G.H., Barnes J. (eds.) Proceedings of the V ADASS Symposium, ASP Conf. Ser. 101, p. 17
- Asai K., Dotani T., Kunieda H., Kawai N., 1996, PASJ 48, L27
- Baan W.A., 1977, ApJ 214, 245
- Baan W.A., 1979, ApJ 227, 987
- Barr P., White N.E., Haberl F., et al., 1987, A&A 176, 69
- Barret D., Olive J.F., Boirin L., et al., 2000, ApJ 533, 329
- Boella G., Butler R.C., Perola G.C., et al., 1997a, A&AS 122, 299
- Boella G., Chiappetti L., Conti G., et al., 1997b, A&AS 122, 327
- Campana S., Stella L., Mereghetti S., et al., 1998, ApJ 499, L65
- Chiappetti L., Dal Fiume D., 1997, In: di Gesù V., Duff M.J.B., Heck A., et al. (eds.) Proceedings of the Fifth International Workshop on Data Analysis in Astronomy. World Scientific Press, p. 101
- Claret A., Goldwurm A., Cordier B., et al., 1994, ApJ 423, 436
- Finger M.H., Koh D.T., Nelson R.W., et al., 1996, Nat 381, 291
- Fiore F., Guainazzi M., Grandi P., 1999, Technical Report 1.2, *BeppoSAX* scientific data center, available online at ftp://www.sdc.asi.it/pub/sax/doc/software_docs/saxabc.v1.2.ps

- Fox D., Lewin W.H.G., 1999, IAU Circ. 7081
- Fox D., Guerriero R., Lewin W.H.G., et al., 1998, ATel² 9
- Frontera F., Costa E., Dal Fiume D., et al., 1997, A&AS 122, 357
- Frontera F., Dal Fiume D., Malaguti G., et al., 1998, Nucl. Phys. B Proc. Suppl. 69, 286
- Gilfanov M., Revnivtsev M., Sunyaev R.A., Churazov E., 1998, A&A 338, L83
- Guerriero R., Fox D., Kommers J., et al., 1999, MNRAS 307, 179
- Illarionov A.F., Sunyaev R.A., 1975, A&A 39, 185
- Kouveliotou C., van Paradijs J., Fishman G.J., et al., 1996, Nat 379, 799
- Lamb F.K., Fabian A.C., Pringle J.E., Lamb D.Q., 1977, ApJ 217, 197
- Lammers U., 1997, The SAX/LECS Data Analysis System User Manual, SAX/LEDA/0010
- Lewin W.H.G., Doty J., Clark G.W., et al., 1976, ApJ 207, L95
- Lewin W.H.G., van Paradijs J., Taam R.E., 1995, In: Lewin W.H.G., van Paradijs J., van den Heuvel E.P.J. (eds.) X-ray Binaries. Cambridge Univ. Press, p. 175
- Lubin L.M., Lewin W.H.G., Rutledge R.E., et al., 1992, MNRAS 258, 759
- Lubin L.M., Lewin W.H.G., van Paradijs J., van der Klis M., 1993, MNRAS 261, 149
- Marshall H.L., Hoffman J.A., Doty J., Lewin W.H.G., Ulmer M.P., 1979, ApJ 227, 555
- Masetti N., Pian E., Frontera F., et al., 2000, five Low Mass X-ray Binaries. In: Malaguti G., Palumbo G.G.C., White N.E. (eds.) Proc. of the Symposium: X-ray Astronomy '999, Gordon and Breach Publishing Group, in press
- Moore C.B., Rutledge R.E., Fox D.W., et al., 2000, ApJ 532, 118
- Morrison R., McCammon D., 1983, ApJ 270, 119
- Ortolani S., Bica E., Barbuy B., 1996, A&A 306, 134
- Osaki Y., 1996, PASJ 108, 39
- Parmar A., Martin D.D.E., Bavdaz M., et al., 1997, A&AS 122, 309
- Stella L., White N.E., Rosner R., et al., 1986, ApJ 308, 669
- Stella L., Haberl F., Lewin W.H.G., et al., 1988, ApJ 324, 379
- Stella L., Campana S., Colpi M., Mereghetti S., Tavani M., 1994, ApJ 423, L47
- Tan J., Lewin W.H.G., Lubin L.M., et al., 1991, MNRAS 251, 1
- Tanaka Y., Shibazaki N., 1996, ARA&A 34, 607
- Tavani M., Barret D., 1997, In: Dermer C.D., Strickman M.S., Kurfess J.D. (eds.) Proc. of the Fourth Compton Symposium. AIP Conf. Proc. 410, p. 75
- Titarchuk L., 1994, ApJ 434, 570
- White N.E., Stella L., Parmar A.N., 1988, ApJ 324, 363

² *The Astronomer's Telegrams* are available online at <http://atel.caltech.edu/>